ATLAS NOTE

ATL-PHYS-PUB-2015-027

25th July 2015

Performance of missing transverse momentum reconstruction with the ATLAS detector in the first proton-proton collisions at $\sqrt{s} = 13$ TeV

The ATLAS Collaboration

Abstract

In June 2015 the Large Hadron Collider restarted collisions at a centre-of-mass energy of 13 TeV. Preliminary studies of the first data collected by the ATLAS experiment, corresponding to an integrated luminosity of about 6 pb^{-1}, offer a good opportunity to test both the performance of the missing transverse momentum ($E_{\mathrm{T}}^{\mathrm{miss}}$) reconstruction with data and its agreement with simulation. $E_{\mathrm{T}}^{\mathrm{miss}}$ is calculated from calibrated and corrected physics objects using a track-based soft term. The $E_{\mathrm{T}}^{\mathrm{miss}}$ performance is studied in two complementary topologies with and without genuine $E_{\mathrm{T}}^{\mathrm{miss}}$, $W \to e\nu$ and $Z \to \mu\mu$. General $E_{\mathrm{T}}^{\mathrm{miss}}$ distributions are shown comparing data with the expectation from the simulated signal and relevant background samples. The $E_{\mathrm{T}}^{\mathrm{miss}}$ resolution and its response as a function of the transverse momentum of the reconstructed Z boson are also studied.

1 Introduction

In collider experiments, conservation of momentum in the plane transverse to the beam axis implies that the transverse momentum of the collision products should sum to zero. Any imbalance is known as "missing transverse momentum", or $E_{\mathrm{T}}^{\mathrm{miss}}$, and may be indicative of weakly-interacting, stable particles in the final state. Within the Standard Model, this arises from neutrinos. There are also prospects for such particles in theories beyond the Standard Model, making $E_{\mathrm{T}}^{\mathrm{miss}}$ an important variable in searches for exotic signatures. Fake $E_{\mathrm{T}}^{\mathrm{miss}}$ can also result from interacting Standard Model particles which escape the acceptance of the detector, are badly reconstructed, or fail to be reconstructed altogether. $E_{\mathrm{T}}^{\mathrm{miss}}$ thus can also serve as an important measure of the overall event reconstruction performance.

$E_{\mathrm{T}}^{\mathrm{miss}}$ reconstructed in 2015 data with a track-based soft term (TST $E_{\mathrm{T}}^{\mathrm{miss}}$) [1] is compared to Monte Carlo (MC) simulations. The reconstructed TST $E_{\mathrm{T}}^{\mathrm{miss}}$ comprises contributions from the "hard term" and the "soft term". The hard term contains selected reconstructed and fully calibrated physics objects. The track-based soft term contains reconstructed tracks associated with the hard-scatter vertex that are not associated to the hard term.

A major difficulty in the $E_{\mathrm{T}}^{\mathrm{miss}}$ reconstruction is its vulnerability to additional proton-proton (pp) interactions which overlap with the hard-scatter process (pile-up). This can come in the form of both in-time pile-up, additional proton-proton collisions in the same bunch crossing, and out-of-time pile-up, which results from interactions from other bunch crossings. Both the hard term and the soft term are affected by pile-up. The objects contributing to the hard term are fully calibrated and corrected for pile-up. For the soft term, several correction methods have been developed in ATLAS to mitigate the effect of pile-up on the $E_{\mathrm{T}}^{\mathrm{miss}}$ reconstruction performance [2], in particular TST $E_{\mathrm{T}}^{\mathrm{miss}}$. Only tracks associated to the identified hard scatter vertex are used for the track-based soft term, making this term robust against pileup.

This note is organized as follows. Section 2 gives a brief description of the ATLAS detector. The data and MC simulation samples are described in Section 3. Section 4 covers the details of $E_{\mathrm{T}}^{\mathrm{miss}}$ reconstruction and the object selections. Section 5 describes the event selection. Finally, Section 6 presents the various $E_{\mathrm{T}}^{\mathrm{miss}}$ distributions and the analysis of $E_{\mathrm{T}}^{\mathrm{miss}}$ performance in data and simulated events.

2 ATLAS detector

The ATLAS experiment [3] at the LHC is a multi-purpose particle detector with a forward-backward symmetric cylindrical geometry and a near 4π coverage in solid angle [1]. It consists of an inner tracking detector (ID) residing in a 2 T axial magnetic field provided by a superconducting solenoid, surrounded by electromagnetic and hadronic calorimetry, and a muon spectrometer. The ID covers the pseudorapidity range $|\eta| < 2.5$, and consists of a silicon pixel detector, a silicon micro-strip detector (SCT) and a transition radiation tracker (TRT) for $|\eta| < 2.0$. During the first LHC long shutdown, a new tracking layer, known as the Insertable B-Layer (IBL) [4], was added close to the beam pipe. The high-granularity lead/liquid-argon (LAr) sampling electromagnetic calorimeter covers the region $|\eta| < 3.2$. The iron/scintillator-tile

[1] ATLAS uses a right-handed coordinate system with its origin at the nominal interaction point (IP) in the centre of the detector and the z-axis along the beam pipe. The x-axis points from the IP to the centre of the LHC ring, and the y-axis points upwards. Cylindrical coordinates (r, ϕ) are used in the transverse plane, ϕ being the azimuthal angle around the z-axis. The pseudorapidity is defined in terms of the polar angle θ as $\eta = -\ln\tan(\theta/2)$. Angular distance is measured in units of $\Delta R \equiv \sqrt{(\Delta\eta)^2 + (\Delta\phi)^2}$.

calorimeter provides hadronic coverage in the central pseudorapidity range $|\eta| < 1.7$. LAr technology is also used for the hadronic calorimeters in the end-cap region $1.5 < |\eta| < 3.2$ and for both electromagnetic and hadronic measurements in the forward region, to $|\eta| < 4.9$. The muon spectrometer (MS) surrounds the calorimeters. It consists of three large superconducting air-core toroid magnets, precision tracking chambers providing accurate muon tracking out to $|\eta| = 2.7$, and additional detectors for triggering in the region $|\eta| < 2.4$. A two-level trigger system is used to select events. There is a low-level hardware trigger which reduces the incoming data rate, and a high-level software trigger which selects interesting final state events.

3 Data and simulation samples

3.1 Data samples

On the 13th and 14th of June 2015, *pp* collisions at a centre-of-mass energy of 13 TeV were recorded with stable proton beams and nominal ATLAS magnetic field conditions. Only data with a fully functioning calorimeter, inner detector and muon spectrometer are analyzed. The standard detector quality criteria are applied, which reduce the impact of instrumental noise and out-of-time calorimeter deposits from cosmic ray and beam backgrounds. The data sample used corresponds to a total integrated luminosity of approximately 6 pb^{-1}, collected with a bunch crossing interval (bunch spacing) of 50 ns. The uncertainty on the integrated luminosity is 9%. It is derived, following a methodology similar to that detailed in [5], from a preliminary calibration of the luminosity scale using a pair of $x - y$ beam-separation scans performed in June 2015. The average number of interactions per bunch crossing in the data sample is $< \mu >= 19$.

3.2 Monte Carlo samples

The MC-simulated events are processed with the GEANT4 software toolkit [6] that simulates the propagations of the generated particles through the ATLAS detector and their interactions with the detector material [7]. The $Z \to \ell\ell$ and $W \to \ell\nu$ samples are generated by POWHEG [8] interfaced to PYTHIA8 [9] and using the AZNLO [10] tune. The $t\bar{t}$ sample uses POWHEG interfaced to PYTHIA6 [11] and the Perugia2012 [12] tune, with the cross-section calculated at NLLO in QCD including resummation of NNLL soft gluon terms with top++2.0 [13]. Parton distribution functions (PDFs) for the POWHEG + PYTHIA samples are taken from CTEQ6L1 [14]. The pile-up collisions are generated with PYTHIA8 using the MSTW2008 LO PDF [15] and the ATLAS A2 tune [14]. The pile-up interactions are randomly selected for each event, and they are overlaid on the simulated physics process before running event reconstruction. For this overlay, a 50 ns bunch distance is assumed. The reconstruction of simulated events proceeds as with data events. The MC simulation samples are weighted such that the distribution of the average number of interactions per bunch crossing matches that observed in the data sample, to ensure that the pile-up interactions are accurately described. The MC samples are normalized to the corresponding cross-sections, and the sum of the MC simulation is normalized to the number of data events.

4 $E_{\mathrm{T}}^{\mathrm{miss}}$ reconstruction and object selection

4.1 $E_{\mathrm{T}}^{\mathrm{miss}}$ reconstruction

The $E_{\mathrm{T}}^{\mathrm{miss}}$ reconstruction uses selected calibrated hard objects to measure the missing transverse momentum in an event. The $E_{x(y)}^{\mathrm{miss}}$ components are calculated as:

$$E_{x(y)}^{\mathrm{miss}} = E_{x(y)}^{\mathrm{miss},\,e} + E_{x(y)}^{\mathrm{miss},\,\gamma} + E_{x(y)}^{\mathrm{miss},\,\tau} + E_{x(y)}^{\mathrm{miss,\,jets}} + E_{x(y)}^{\mathrm{miss},\,\mu} + E_{x(y)}^{\mathrm{miss,\,soft}}, \tag{1}$$

where each object term is given by the negative vectorial sum of the momenta of the respective calibrated objects described in the following sections. Calorimeter signals are associated with these reconstructed objects in the following order: electrons (e), photons (γ), hadronically decaying τ-leptons, jets and muons (μ). The soft term is reconstructed from detector signal objects not associated with any object passing the above selection cuts. These can be ID tracks (track-based soft term) or calorimeter signals (calorimeter-based soft term). For the studies presented here, only the track-based soft term is considered.

From the components $E_{x(y)}^{\mathrm{miss}}$, the azimuthal angle $\phi^{\mathrm{miss}}$and the magnitude of $E_{\mathrm{T}}^{\mathrm{miss}}$ are calculated as:

$$E_{\mathrm{T}}^{\mathrm{miss}} = \sqrt{(E_x^{\mathrm{miss}})^2 + \left(E_y^{\mathrm{miss}}\right)^2}, \tag{2}$$

$$\phi^{\mathrm{miss}} = \arctan\left(E_y^{\mathrm{miss}}/E_x^{\mathrm{miss}}\right). \tag{3}$$

An important quantity to estimate the event activity is ΣE_{T}, which is defined as the scalar sum of transverse momenta of the hard objects and soft term contributions :

$$\Sigma E_{\mathrm{T}} = \sum p_{\mathrm{T}}^{e} + \sum p_{\mathrm{T}}^{\gamma} + \sum p_{\mathrm{T}}^{\tau} + \sum p_{\mathrm{T}}^{\mathrm{jets}} + \sum p_{\mathrm{T}}^{\mu} + \sum p_{\mathrm{T}}^{\mathrm{soft}}. \tag{4}$$

4.2 Object selection

The following selections are applied to physics objects used for the $E_{\mathrm{T}}^{\mathrm{miss}}$ reconstruction [1].

4.2.1 Track and Vertex Selection

Hits in the ID are used to reconstruct tracks pointing to a particular collision vertex [16, 17]. Both tracks and vertices are required to pass basic quality cuts: tracks are required to have $p_{\mathrm{T}} > 0.4\,\mathrm{GeV}$ and $|\eta| < 2.5$, in addition to reconstruction quality requirements [18] . Vertices are required to pass cuts on the transverse (longitudinal) impact parameter $d_0 < 1.5$ cm ($z_0 < 1.5$ cm) , and those tracks used to reconstruct vertices must pass requirements on the number of hits in the ID. The vertex with highest Σp_{T}^2, summed over all tracks associated with it, is called the primary vertex and generally corresponds to the hard-scatter vertex.

4.2.2 Muon Selection

Muons are selected according to the "Medium" recommendation, similar to those criteria used in Run 1 [19]. Muons are required to have $p_{\mathrm{T}} > 10\,\mathrm{GeV}$. Muons with associated ID tracks are reconstructed within $|\eta| < 2.5$, while those in the region $2.5 < |\eta| < 2.7$ are reconstructed in the muon spectrometer only, with tightened requirements on the number of MS track hits.

4.2.3 Electron Selection

Electrons are selected based on their association between calorimeter clusters and ID tracks, which is evaluated using a likelihood-based criterion [20]. The electrons in this note are selected using the "Medium" recommendation. Electrons are calibrated using the default calibration given in [21], and are required to have $p_{\mathrm{T}} > 10\,\mathrm{GeV}$ $|\eta| < 1.37$ or $1.52 < |\eta| < 2.47$ to avoid the transition region between the central and end-cap electromagnetic calorimeters.

4.2.4 Photon Selection

The identification of photons exploits the distinctive evolution of their electromagnetic showers [22]. Photons are selected and calibrated [21] using the "Tight" recommendation. Photons must have $p_{\mathrm{T}} > 25\,\mathrm{GeV}$ and $|\eta| < 1.37$ or $1.52 < |\eta| < 2.37$ to avoid the transition region between the central and end-cap electromagnetic calorimeters.

4.2.5 Tau Selection

In ATLAS, hadronically-decaying τ-leptons are principally reconstructed from narrow jets with low track multiplicities. τ-lepton candidates must pass the "Medium" recommendation [23], with $p_{\mathrm{T}} > 20\,\mathrm{GeV}$ and $|\eta| < 1.37$ or $1.52 < |\eta| < 2.37$ to avoid the transitionregion between the central and end-cap electromagnetic calorimeters.

4.2.6 Jet Selection

Jets are reconstructed from clusters of topologically connected cells in the calorimeter. These "topo-clusters" are calibrated at the electromagnetic energy scale [2]. The anti-k_t algorithm [24] with distance parameter $R = 0.4$ is employed, as provided by the FastJet toolkit [25]. The jets are fully calibrated using the EM+JES scheme [18] and a correction for pile-up [26], and required to have calibrated $p_{\mathrm{T}} > 20\,\mathrm{GeV}$. To remove jets originating from pile-up, a cut on the jet vertex tagger variable (JVT) [27] of JVT > 0.64 is applied to jets with $|\eta| < 2.4$ and $p_{\mathrm{T}} < 50\,\mathrm{GeV}$ included in reconstruction of TST $E_{\mathrm{T}}^{\mathrm{miss}}$. The primary vertex associated tracks from jets which fail these quality requirements are included in the TST $E_{\mathrm{T}}^{\mathrm{miss}}$ soft term.

[2] This scale provides a good representation of the electron or photon energy in the calorimeter, but does not correct for energy losses associated with hadronic showers.

4.3 $E_{\mathrm{T}}^{\mathrm{miss}}$ soft term

Several algorithms have been developed to measure the $E_{\mathrm{T}}^{\mathrm{miss}}$ soft term. Methods aimed at reducing the impact of pile-up interactions make use of ID tracks, which can be matched to the primary vertex corresponding to the hard interaction [2]. Here we describe the track-based soft term, which is used in the reconstruction of TST $E_{\mathrm{T}}^{\mathrm{miss}}$ [1].

4.3.1 Track Soft Term

The track soft term is built from tracks satisfying the selection described in Sect. 4.2.1 but not matched to any hard object. Only those tracks associated with the primary vertex through requirements on the longitudinal and transverse impact parameters are included. The overlap removal between tracks and calorimeter clusters associated to the high-p_{T} objects used in the TST is summarized as follows:

- Tracks within ΔR(track, electron/photon cluster) < 0.05 are removed.
- Tracks within ΔR(track, τ-lepton) < 0.2 are removed.
- ID tracks associated to combined or segment-tagged muons are replaced with the combined ID+MS fit.
- Tracks associated with jets using the ghost-association technique [28, 29] are removed.

Furthermore, tracks with momentum uncertainties larger than 40% are removed. Since tracks can be matched to a primary vertex, TST $E_{\mathrm{T}}^{\mathrm{miss}}$ is relatively insensitive to pile-up effects but does not include contributions from soft neutral particles.

5 Event selection

5.1 $Z \to \mu\mu$ event selection

$Z \to \mu\mu$ events provide an ideal final state for the evaluation of $E_{\mathrm{T}}^{\mathrm{miss}}$ performance, due to the limited backgrounds and precise measurement of the kinematics of the Z boson. Neutrinos are produced only through heavy-flavour meson decays, so this channel has very little genuine $E_{\mathrm{T}}^{\mathrm{miss}}$, making the resolution measured by the width of the $E_{x(y)}^{\mathrm{miss}}$ distribution indicative of the $E_{\mathrm{T}}^{\mathrm{miss}}$ reconstruction quality. The offline selection of $Z \to \mu\mu$ events requires exactly two muons, as defined in Sect. 4.2.2, with the following additional criteria: the muons must have opposite charge and $p_{\mathrm{T}} > 25\,\mathrm{GeV}$, and the reconstructed invariant mass of the dimuon system, $m_{\ell\ell}$, is required to be consistent with the mass of the Z boson, $|m_{\ell\ell} - m_Z| < 25\,\mathrm{GeV}$.

5.2 $W \to e\nu$ event selection

$W \to e\nu$ events provide an important event topology with neutrinos from the hard-scatter interaction. The genuine $E_{\mathrm{T}}^{\mathrm{miss}}$ is caused by the neutrino transverse momentum $p_T^{\nu} > 0$, and provides a good metric to validate the scale and direction (azimuth) of the reconstructed $E_{\mathrm{T}}^{\mathrm{miss}}$. Candidate $W \to e\nu$ events are required to pass the high-level loose electron trigger with $p_{\mathrm{T}} > 17\,\mathrm{GeV}$. Electron candidates are selected based on criteria described in Sect. 4.2.3. Events are required to contain exactly one electron. Selections on the $E_{\mathrm{T}}^{\mathrm{miss}}$ and reconstructed transverse mass are used to reduce the multijet background with one jet emulating an isolated electron from the W boson. TST $E_{\mathrm{T}}^{\mathrm{miss}}$, calculated as described in Sect. 4, is required to be greater than 25 GeV.

The reconstructed transverse mass of the electron and the TST $E_{\mathrm{T}}^{\mathrm{miss}}$ is defined as:

$$m_{\mathrm{T}} = \sqrt{2p_{\mathrm{T}}^{\ell}E_{\mathrm{T}}^{\mathrm{miss}}(1 - \cos\Delta\phi)}, \tag{5}$$

where p_{T}^{ℓ} is the transverse momentum of the electron and $\Delta\phi$ is the azimuthal angle between the electron momentum and $\vec{E}_{\mathrm{T}}^{\mathrm{miss}}$. The transverse mass is required to be greater than 50 GeV.

6 Performance of missing transverse momentum in data and MC simulation

6.1 Data to MC comparisons for $Z \to \mu\mu$ and $W \to e\nu$ events

In this section, the performance of TST $E_{\mathrm{T}}^{\mathrm{miss}}$ reconstruction in $Z \to \mu\mu$ and $W \to e\nu$ data events is compared with the expected performance from the MC samples for the signal and the relevant background processes.

6.1.1 $Z \to \mu\mu$ events

$Z \to \mu\mu$ events are used to study the $E_{\mathrm{T}}^{\mathrm{miss}}$ performance in events in which no genuine $E_{\mathrm{T}}^{\mathrm{miss}}$ is expected. About 4000 events in data pass the $Z \to \mu\mu$ selection and the agreement with the MC simulation is studied. Fig. 1 shows the distributions of $E_{\mathrm{T}}^{\mathrm{miss}}$, ΣE_{T}, $E_{\mathrm{x}}^{\mathrm{miss}}$, $E_{\mathrm{y}}^{\mathrm{miss}}$ for TST $E_{\mathrm{T}}^{\mathrm{miss}}$. Fig. 2 shows $E_{\mathrm{T}}^{\mathrm{miss}}$ distributions for the jet, muons and soft terms for TST $E_{\mathrm{T}}^{\mathrm{miss}}$. The agreement in the bulk of the distributions is within 20%. In the high $E_{\mathrm{T}}^{\mathrm{miss}}$ and ΣE_{T} regions the data deviate somewhat from the background expectation but the statistical precision of the data is limited. The feature at zero in the jet term TST $E_{\mathrm{T}}^{\mathrm{miss}}$ is due to events with no jets. Diboson background samples are not included in these studies due to the small number of expected events given the limited luminosity [30].

6.1.2 $W \to e\nu$ events

$W \to \ell\nu$ events allow the evaluation of the performance of the $E_{\mathrm{T}}^{\mathrm{miss}}$ reconstruction in events in which genuine $E_{\mathrm{T}}^{\mathrm{miss}}$ is expected due to the neutrino. About 40000 events in data pass the $W \to e\nu$ selection and the agreement with the MC simulation is studied. Fig. 3 shows the overall TST $E_{\mathrm{T}}^{\mathrm{miss}}$ distribution and the soft term of the TST $E_{\mathrm{T}}^{\mathrm{miss}}$. The agreement between data and MC simulation is worse with respect to the

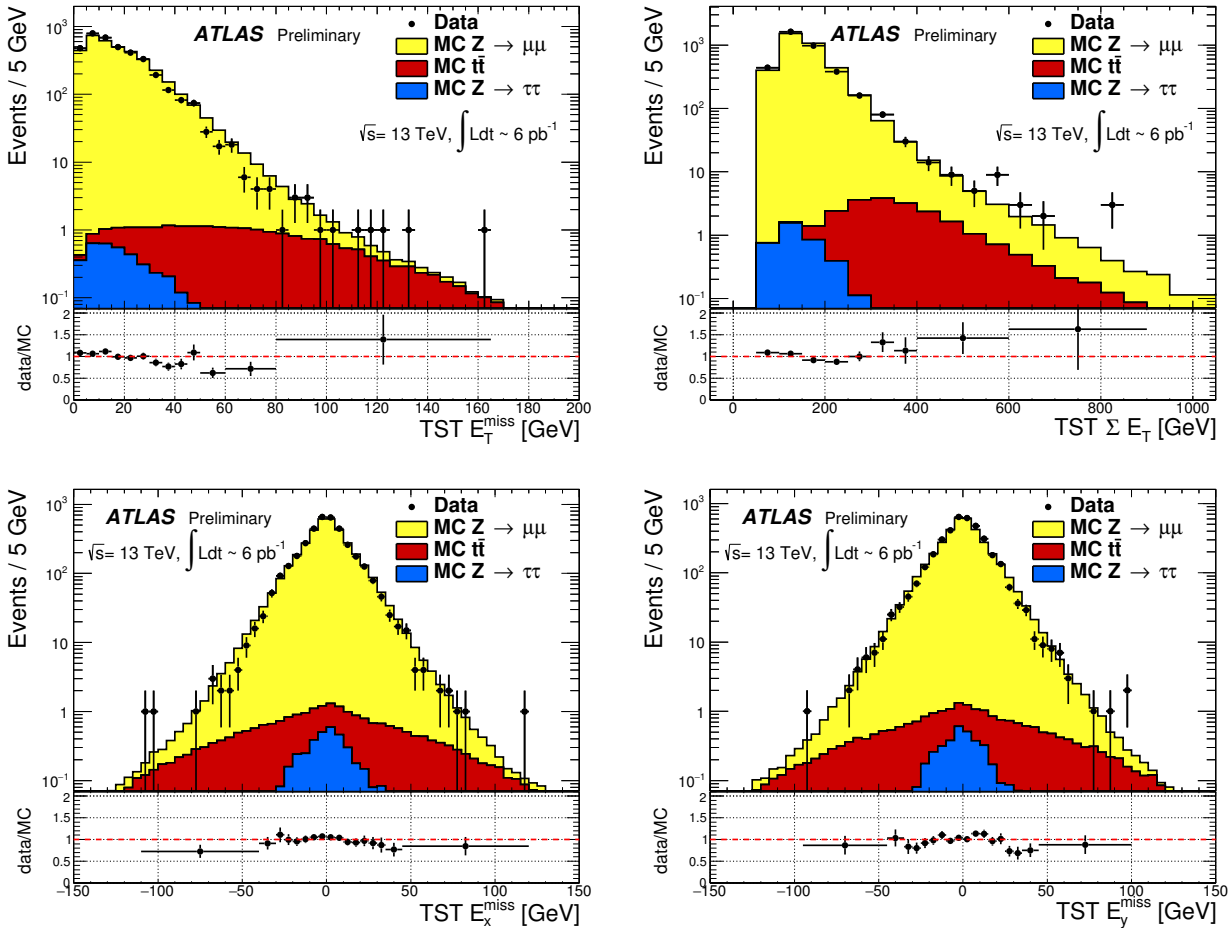

Figure 1: Distributions of TST $E_{\mathrm{T}}^{\mathrm{miss}}$, ΣE_{T}, $E_{\mathrm{x}}^{\mathrm{miss}}$, $E_{\mathrm{y}}^{\mathrm{miss}}$ in $Z \to \mu\mu$ events. The expectation from MC simulation is superimposed and normalized to data, after each MC sample is weighted with its corresponding cross-section.

$Z \to \mu\mu$ events in the low $E_{\mathrm{T}}^{\mathrm{miss}}$ region; this is likely due to the multi-jet background which is not included in the MC simulation. Diboson and $W \to \tau\nu$ background samples are also not included in these studies due to the small number of expected events given the limited luminosity [30].

6.2 $E_{\mathrm{T}}^{\mathrm{miss}}$ resolution

The $E_{\mathrm{T}}^{\mathrm{miss}}$ resolution is evaluated in $Z \to \mu\mu$ data and MC events in which no genuine $E_{\mathrm{T}}^{\mathrm{miss}}$ is expected. The resolution is plotted as a function of the ΣE_{T} in the event, calculated using the calorimeter-based soft term, and as a function of the number of primary vertices. The choice of the calorimeter-based soft term allows comparisons with other studies [30] [3]. The value of the resolution in each bin is estimated from the

[3] Direct comparisons with past studies [30] are not straightforward. Previous studies defined each bin of the resolution as the standard deviation of a fit to a Gaussian distribution. To allow comparisons with versions of $E_{\mathrm{T}}^{\mathrm{miss}}$ based on tracking, with non-Gaussian tails, the root-mean square is used instead. The resolution defined using the root-mean square is thus strictly larger than the resolution used in past studies. In addition, the algorithms used in $E_{\mathrm{T}}^{\mathrm{miss}}$ reconstruction have changed. For comparisons between Run 1 and Run 2 algorithms using the same performance definitions refer to Ref. [1].

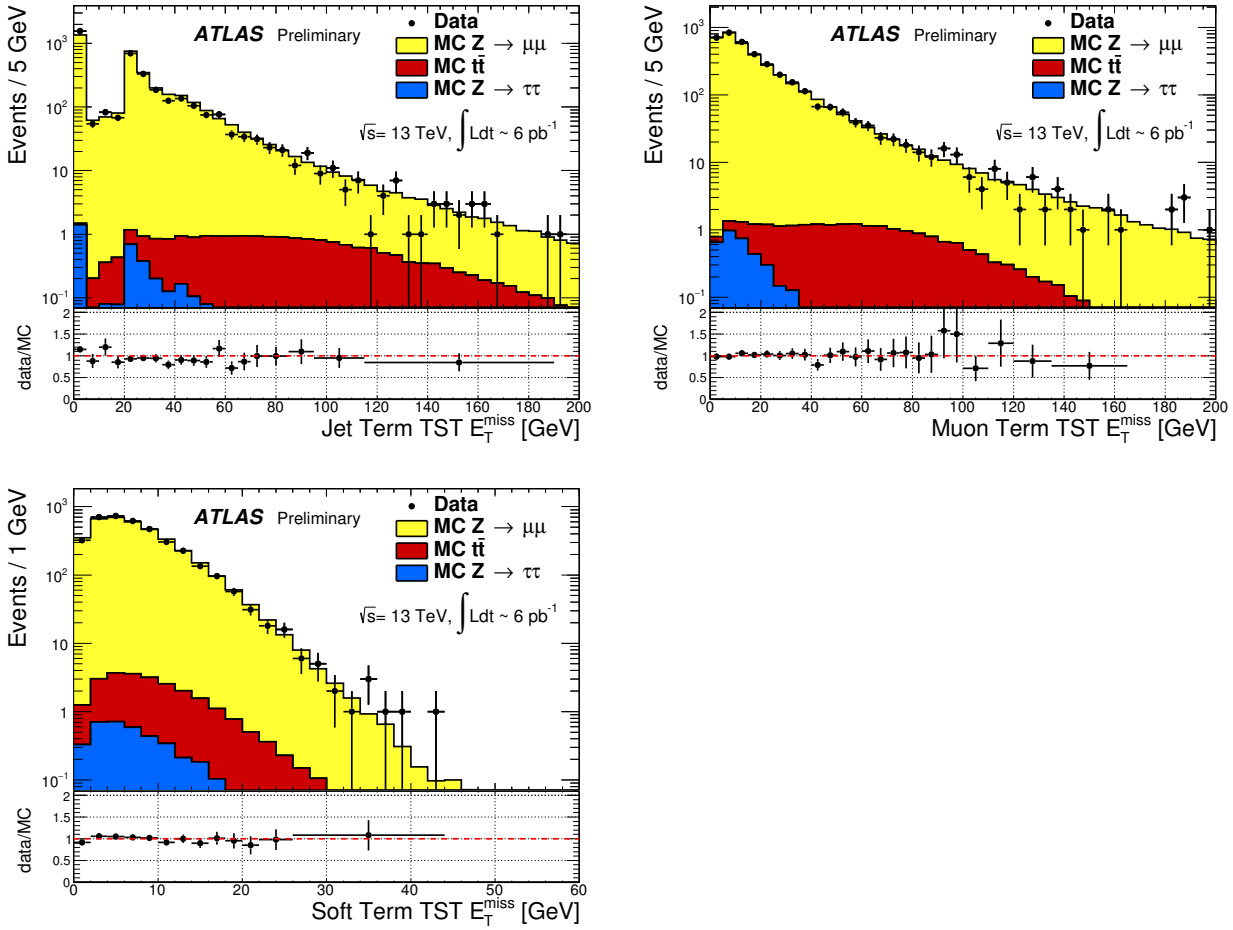

Figure 2: Distributions of jet term, muon term and soft term for TST $E_{\mathrm{T}}^{\mathrm{miss}}$ in $Z \to \mu\mu$ events. The expectation from MC simulation is superimposed and normalized to data, after each MC sample is weighted with its corresponding cross-section.

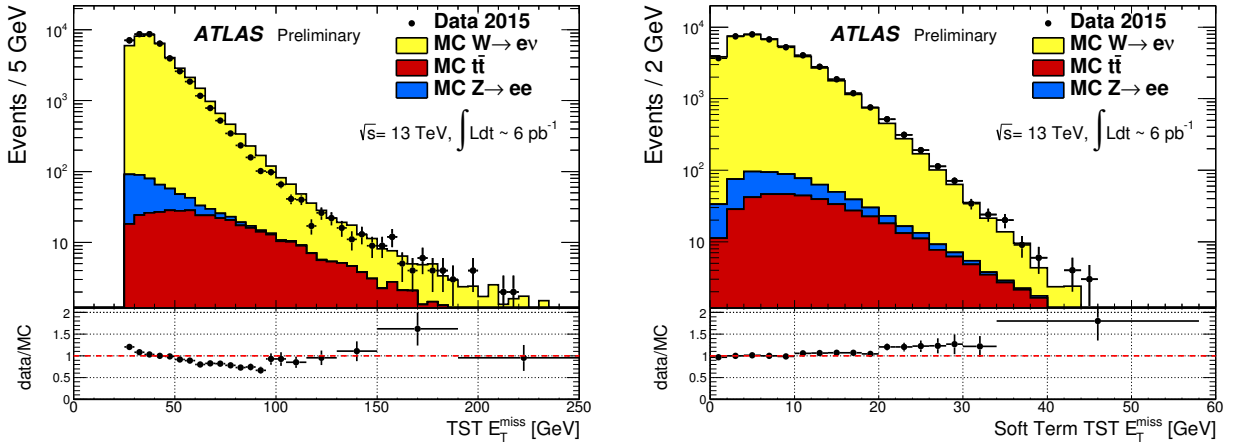

Figure 3: Distributions of TST total and soft term $E_{\mathrm{T}}^{\mathrm{miss}}$ in $W \to e\nu$ events. The expectation from MC simulation is superimposed and normalized to data, after each MC sample is weighted with its corresponding cross-section.

root-mean square of the combined of $E_{\mathrm{x}}^{\mathrm{miss}}$ and $E_{\mathrm{y}}^{\mathrm{miss}}$ in bins of ΣE_{T} (number of primary vertices). Each bin is required to have a minimum of 200 events to be considered for the resolution curve. Reasonable agreement is found between data and MC simulation, considering the low statistics available in data.

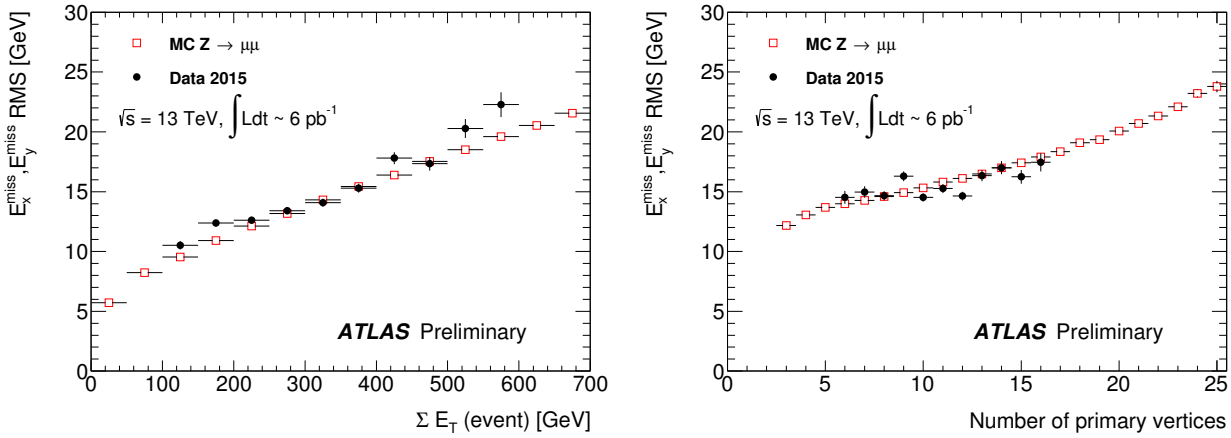

Figure 4: Distributions of TST $E_{\mathrm{x}}^{\mathrm{miss}}$, $E_{\mathrm{y}}^{\mathrm{miss}}$ resolution as a function of ΣE_{T} and of the number of primary vertices in $Z \to \mu\mu$ events. The data (black circles) and MC simulation (red squares) are overlaid.

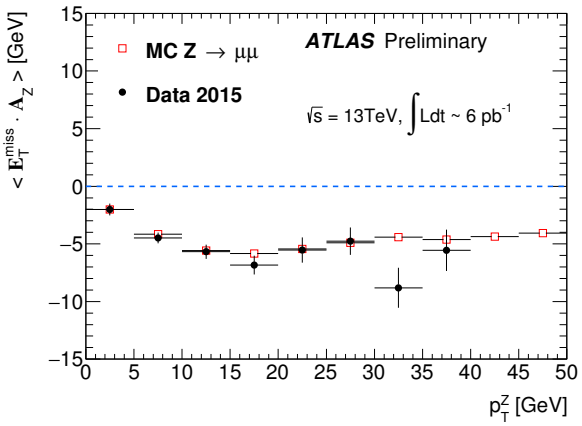

Figure 5: Distribution of TST $E_{\mathrm{T}}^{\mathrm{miss}}$ scale as a function of p_{T}^{Z} in $Z \to \mu\mu$ events. The data (black circles) and MC simulation (red squares) are overlaid.

6.3 $E_{\mathrm{T}}^{\mathrm{miss}}$ scale

In events with $Z \to \mu\mu$ decays, the p_{T} of the Z boson defines an axis in the transverse plane of the ATLAS detector. The component of the $E_{\mathrm{T}}^{\mathrm{miss}}$ along the $\mathbf{p}_{\mathrm{T}}^{Z}$ axis is sensitive to biases in detector responses. The unit vector of $\mathbf{p}_{\mathrm{T}}^{Z}$ is labeled as A_Z, and it is defined as:

$$A_Z = \frac{\vec{p_T}^{\,\ell^+} + \vec{p_T}^{\,\ell^-}}{|\vec{p_T}^{\,\ell^+} + \vec{p_T}^{\,\ell^-}|}, \tag{6}$$

where $\vec{p_T}^{\ell^+}$ and $\vec{p_T}^{\ell^-}$ are the transverse momenta of the leptons from the Z boson decay.

The mean value of the $E_{\mathrm{T}}^{\mathrm{miss}}$ projected onto $\boldsymbol{A}_Z$, $\langle \vec{E}_{\mathrm{T}}^{\mathrm{miss}} \cdot \boldsymbol{A}_Z \rangle$, is a measure of the $E_{\mathrm{T}}^{\mathrm{miss}}$ scale, as this axis is sensitive to the balance between the hard objects and the soft hadronic recoil. If the hard objects are perfectly balanced against the soft hadronic recoil, the projection of $E_{\mathrm{T}}^{\mathrm{miss}}$ onto $\boldsymbol{A}_Z$ would be zero, independent of p_{T}^Z. Fig. 5 shows the $E_{\mathrm{T}}^{\mathrm{miss}}$ scale for data and MC simulation. Each bin is required to have a minimum of 200 events to be considered in the scale plot. The negative bias of about 5 GeV likely indicates an underestimation of the TST $E_{\mathrm{T}}^{\mathrm{miss}}$ from two sources: the TST $E_{\mathrm{T}}^{\mathrm{miss}}$ does not include contributions from the soft neutral particles and the limited acceptance of the ID. The agreement is good between the data and MC simulation, other than some fluctuations for high p_{T}^Z events, due to low statistics.

7 Conclusion

The performance and reconstruction of the missing transverse momentum in the first 13 TeV collision data has been studied, and compared to MC simulation samples, for events with and without genuine $E_{\mathrm{T}}^{\mathrm{miss}}$. Reasonable agreement between data and MC simulation is observed in the $E_{\mathrm{T}}^{\mathrm{miss}}$ distributions for $Z \to \mu\mu$ events, while there are some discrepancies observed in $W \to e\nu$ events. The agreement of the $E_{\mathrm{T}}^{\mathrm{miss}}$ resolution (scale) is acceptable given the limited accessible ΣE_{T} (p_{T}^Z) range, which arises from the limited number of events available in data.

References

[1] ATLAS Collaboration, *Expected performance of missing transverse momentum reconstruction for the ATLAS detector at $\sqrt{s}$ = 13 TeV*, ATL-PHYS-PUB-2015-023 (2015), URL: https://cds.cern.ch/record/2013489/.

[2] ATLAS Collaboration, *Pile-up Correction in Missing Transverse Momentum Reconstruction in the ATLAS Experiment in Proton-Proton Collisions at $\sqrt{s}$ = 8 TeV*, ATLAS-CONF-2014-019 (2014), URL: https://cds.cern.ch/record/1702055.

[3] ATLAS Collaboration, *The ATLAS Experiment at the CERN Large Hadron Collider*, JINST **3** (2008) S08003.

[4] M Capeans et al., *ATLAS Insertable B-Layer Technical Design Report*, CERN-LHCC-2010-013. ATLAS-TDR-19 (2010), URL: https://cds.cern.ch/record/1291633.

[5] G. Aad et al., *Improved luminosity determination in pp collisions at sqrt(s) = 7 TeV using the ATLAS detector at the LHC*, Eur.Phys.J. **C73**.8 (2013) 2518, arXiv: 1302.4393 [hep-ex].

[6] S. Agostinelli et al., *GEANT4: A simulation toolkit*, Nucl. Instrum. Meth. **A506** (2003) 250–303.

[7] ATLAS Collaboration, *The ATLAS Simulation Infrastructure*, Eur. Phys. J. C **70** (2010) 823, arXiv: 1005.4568 [hep-ex].

[8] S. Frixione, P. Nason and C. Oleari, *Matching NLO QCD computations with parton shower simulations :the POWHEG method*, JHEP **11** (2007) 070.

[9] T. Sjostrand, S. Mrenna and P. Z. Skands, *A Brief Introduction to PYTHIA 8.1*, Comput. Phys. Commun. **178** (2008) 852–867, arXiv: 0710.3820 [hep-ph].

[10] ATLAS Collaboration, *Measurement of the Z/γ^* boson transverse momentum distribution in pp collisions at $\sqrt{s} = 7$ TeV with the ATLAS detector* , JHEP **1409** (2014) 145, arXiv: 1406.3660 [hep-ph].

[11] T. Sjostrand, S. Mrenna and P. Z. Skands, *PYTHIA 6.4 Physics and Manual*, JHEP **0605** (2006) 026, arXiv: hep-ph/0603175 [hep-ph].

[12] P. Z. Skands, *Tuning Monte Carlo generators: The Perugia tunes*, Phys. Rev. D **82** (7 2010) 074018, URL: http://link.aps.org/doi/10.1103/PhysRevD.82.074018.

[13] M. Czakon and A. Mitov, *A new method for combining NLO QCD with shower Monte Carlo algorithms*, Computer Physics Communications **185** (2014) 2930–2938, arXiv: hep-ph/1112.5675 [hep-ph].

[14] ATLAS Collaboration, *Further ATLAS tunes of Pythia 6 and Pythia 8*, ATL-PHYS-PUB-2011-014 (2011), eprint: https://cds.cern.ch/record/1400677.

[15] A. Martin et al., *Parton distributions for the LHC*, Eur.Phys.J. **C63** (2009) 189–285, arXiv: 0901.0002 [hep-ph].

[16] ATLAS Collaboration, *Alignment of the ATLAS Inner Detector and its Performance in 2012*, ATLAS-CONF-2014-047 (2014), URL: https://cds.cern.ch/record/1741021.

[17] ATLAS Collaboration, *Performance of the ATLAS Inner Detector Track and Vertex Reconstruction in the High Pile-Up LHC Environment*, ATLAS-CONF-2012-042 (2012), URL: https://cds.cern.ch/record/1435196.

[18] ATLAS Collaboration, *Data-driven determination of the energy scale and resolution of jets reconstructed in the ATLAS calorimeters using dijet and multijet events at $\sqrt{s} = 8$ TeV*, ATLAS-CONF-2015-017 (2015), URL: https://cds.cern.ch/record/2008678.

[19] ATLAS Collaboration, *Measurement of the muon reconstruction performance of the ATLASdetector using 2011 and 2012 LHC proton-proton collision data*, Eur. Phys. J. **C74** (2014) 3130, arXiv: 1407.3935 [hep-ex].

[20] ATLAS Collaboration, *Electron efficiency measurements with the ATLAS detector using the 2012 LHC proton-proton collision data*, ATLAS-CONF-2014-032 (2014), URL: http://cdsweb.cern.ch/record/1706245.

[21] ATLAS Collaboration, *Electron and photon energy calibration with the ATLAS detector using LHC Run 1 data*, Eur. Phys. J. **C74**.10 (2014) 3071, arXiv: 1407.5063 [hep-ex].

[22] ATLAS Collaboration, *Measurements of the photon identification efficiency with the ATLAS detector using 4.9 fb^{-1} of pp collision data collected in 2011*, ATLAS-CONF-2012-123 (2012), URL: http://cdsweb.cern.ch/record/1473426.

[23] ATLAS Collaboration, *Identification and energy calibration of hadronically decaying tau leptons with the ATLAS experiment in pp collisions at $\sqrt{s} = 8$ TeV*, Eur. Phys. J. **C75** (2015), arXiv: 1412.7086 [hep-ex], URL: https://cds.cern.ch/record/1978197.

[24] M. Cacciari, G. P. Salam and G. Soyez, *The Anti-k(t) jet clustering algorithm*, JHEP **0804** (2008) 063, arXiv: 0802.1189 [hep-ph].

[25] ATLAS Collaboration, *Jet energy measurement with the ATLAS detector in proton–proton collisions at* $\sqrt{s} = 7$ *TeV*, Eur. Phys. J. C **73** (2013) 2304, arXiv: 1112.6426 [hep-ex].

[26] ATLAS Collaboration, *Jet Calibration and Systematic Uncertainties for Jets Reconstructed in the ATLAS Detector at* $\sqrt{s} = 13$ *TeV*, ATL-COM-PHYS-2015-444 (2015), URL: https://cds.cern.ch/record/2018215.

[27] ATLAS Collaboration, *Tagging and suppression of pileup jets with the ATLAS detector*, ATLAS-CONF-2014-018 (2014), URL: https://cds.cern.ch/record/1700870.

[28] M. Cacciari and G. P. Salam, *Pileup subtraction using jet areas*, Phys. Lett. **B659** (2008) 119–126, arXiv: 0707.1378 [hep-ph].

[29] M. Cacciari, G. P. Salam and G. Soyez, *The Catchment Area of Jets*, JHEP **0804** (2008) 005, arXiv: 0802.1188 [hep-ph].

[30] ATLAS Collaboration, *Performance of Missing Transverse Momentum Reconstruction in ATLAS studied in Proton–Proton Collisions recorded in 2012 at* $\sqrt{s} = 8$ *TeV*, ATLAS-CONF-2013-082 (2013), URL: http://cdsweb.cern.ch/record/1570993.